HHS Public Access

Author manuscript

Matrix Biol. Author manuscript; available in PMC 2016 March 01.

Published in final edited form as:

Matrix Biol. 2015 March ; 42: 56–73. doi:10.1016/j.matbio.2014.12.002.

Regulatory mechanisms of anthrax toxin receptor 1-dependent vascular and connective tissue homeostasis

Tatiana Y. Besschetnova[a], **Takaharu Ichimura**[b], **Negin Katebi**[a], **Brad St. Croix**[c], **Joseph V. Bonventre**[b,d], and **Bjorn R. Olsen**[a,e]

[a]**Department of Developmental Biology,** Harvard School of Dental Medicine, USA

[b]**Renal Division,** Department of Medicine, Brigham and Women's Hospital, USA

[c]**Tumor Angiogenesis Section,** Mouse Cancer Genetics Program, National Cancer Institute (NCI), National Institutes of Health (NIH), Frederick, MD USA

[d]**Harvard-MIT Division of Health Sciences and Technology,** USA

[e]**Department of Cell Biology,** Harvard Medical School, USA

Abstract

It is well known that angiogenesis is linked to fibrotic processes in fibroproliferative diseases, but insights into pathophysiological processes are limited, due to lack of understanding of molecular mechanisms controlling endothelial and fibroblastic homeostasis. We demonstrate here that the matrix receptor anthrax toxin receptor 1 (ANTXR1), also known as tumor endothelial marker 8 (TEM8), is an essential component of these mechanisms. Loss of TEM8 function in mice causes reduced synthesis of endothelial basement membrane components and hyperproliferative and leaky blood vessels in skin. In addition, endothelial cell alterations in mutants are almost identical to those of endothelial cells in infantile hemangioma lesions, including activated VEGF receptor signaling in endothelial cells, increased expression of the downstream targets VEGF and CXCL12, and increased numbers of macrophages and mast cells. In contrast, loss of TEM8 in fibroblasts leads to increased rates of synthesis of fiber-forming collagens, resulting in progressive fibrosis in skin and other organs. Compromised interactions between TEM8-deficient endothelial and fibroblastic cells cause dramatic reduction in the activity of the matrix-degrading enzyme MMP2. In addition to insights into mechanisms of connective tissue homeostasis, our data provide molecular explanations for vascular and connective tissue abnormalities in GAPO syndrome,

Correspondence to Tatiana Y. Besschetnova and Bjorn R. Olsen: Harvard School of Dental Medicine, 188 Longwood Avenue, REB 409/406, Boston, MA 02115, USA. Tatiana_Besschetnova@hms.harvard.edu; Bjorn_Olsen@hms.harvard.edu.

Supplementary data to this article can be found online at http://dx.doi.org/10.1016/j.matbio.2014.12.002.

Author contributions

T.Y.B. and B.R.O. designed project, T.Y.B. performed experiments, collected and analyzed data. T.Y.B. and T.I. conducted radiolabeling L-[^{14}C(U)]-Proline experiments. N.K. isolated mouse embryos and did LacZ staining of embryos at different developmental stages. B.S.C. provided Tem8 *fl/fl* mice and J.V.B provided reagents. T.Y.B. and B.R.O. wrote the paper. All authors read, contributed to discussion and approved the final manuscript.

Competing financial interests

The authors declare no competing financial interests.

caused by loss-of-function mutations in *ANTXR1*. Furthermore, the loss of MMP2 activity suggests that fibrotic skin abnormalities in GAPO syndrome are, in part, the consequence of pathophysiological mechanisms underlying syndromes (NAO, Torg and Winchester) with multicentric skin nodulosis and osteolysis caused by homozygous loss-of-function mutations in MMP2.

Keywords

Hemangioma; Angiogenesis; Fibrosis; GAPO syndrome; MMP2

Introduction

Dysregulation of fibrous connective tissues in fibroproliferative diseases is a leading cause of morbidity and mortality in developed countries with about 45% of deaths attributed to such disorders [1]. Alterations in vascular remodeling and angiogenesis are associated with fibrotic processes in different organs [2–5], and systemic sclerosis is correlated with progressive disappearance of blood vessels in the skin [6]. Recently, it has been reported that high levels of vascular endothelial growth factor A (VEGF) aggravates fibrosis in experimental animal models and stimulates collagen production by cultured fibro-blasts isolated from the skin of systemic sclerosis patients [7]. Understanding how such VEGF activities can be reconciled with the disappearance of skin blood vessels during progression of fibrosis in vivo, is problematic without deeper insights into molecular mechanisms responsible for regulating interactions between endothelial and fibroblastic cells, inflammatory cells and macrophages in physiological connective tissue homeostasis.

For several reasons, studies of the receptor ANTXR1 [8–11], also known as TEM8 [12]; are likely to provide such insights. In vitro data suggest that TEM8 has a role in adhesion, spreading and migration of cells through its interaction with extracellular matrix (ECM) components [13–16]. Expression in different cell types and the existence of at least 5 different splice variants, both with and without transmembrane domains, suggests flexible regulatory functions in different tissues [17]. Abnormal clustering of TEM8 with integrin β1 and vascular endothelial growth factor receptor 2 (VEGFR2) occurs in endothelial cells with in cutaneous infantile hemangiomas, the most common vascular anomaly in childhood. Appearing soon after birth, hemangiomas grow rapidly for a few months. This is followed by a period of involution and replacement of the endothelium by fibro-fatty tissue, sometimes leaving disfiguring scars. Finally, in patients with the recessive GAPO syndrome, loss-of-function mutations in TEM8 result ingrowth retardation and bone defects in addition to hemangioma-like vascular anomalies in skin and progressive fibrosis of several organs, including skin [18].

Hemangiomas are discrete lesions and the cutaneous changes in GAPO syndrome are systemic in nature. However, the similarities between the vascular and connective tissue defects in the two disorders suggest that the responsible molecular mechanisms have common features that are relevant to the regulation of connective tissue homeostasis. To identify the cellular and molecular mechanisms by which TEM8 functions in both vascular

and connective tissues in vivo, we generated and studied *Antxr1* null mice as well as mice with conditional deletion of *Antxr1* in endothelial cells. In addition, we generated mice that are heterozygous for an Ala-to-Thr substitution in the transmembrane domain of TEM8, previously identified in a hemangioma patient as a heterozygous germ-line mutation in TEM8 variants 1, 2 and 4 [17,19]. The results of these studies show for the first time that although TEM8-deficient mice do not have localized vascular hemangiomas, they develop proliferative vessels in skin with cell signaling alterations and cellular changes, such as invasion of macrophages and mast cells that are identical to those seen in human hemangioma lesions. In addition, TEM8-deficient mice exhibit progressive skin fibrosis with increased synthesis of collagens in fibroblasts, contrasted with reduced synthesis of major components of vascular basement membranes. Knock-in mice, carrying the Ala-to-Thr substitution in TEM8, show skin defects consistent with the conclusion that the mutation has a dominant negative effect on TEM8 function. Loss of TEM8 function is also associated with compromised interactions between TEM8-deficient endothelial and fibroblastic cells, resulting in a dramatic reduction of matrix metalloproteinase-2 (MMP2) activity. Our study provides a mechanistic explanation for skin and vascular abnormalities in GAPO syndrome [20–22] and suggests that fibrotic skin abnormalities in GAPO syndrome are, in part, the consequence of pathophysiological mechanisms underlying syndromes with multicentric skin nodulosis and osteolysis caused by homozygous loss-of-function mutations in MMP2 [23–25]. Most importantly, the data demonstrate that TEM8 is an essential regulator of connective tissue homeostasis. TEM8 controls synthesis of major matrix components in both endothelial and fibroblastic cells, it regulates signaling pathways controlling growth factors and chemokines, and it is an essential component of an endothelial-fibroblastic interaction mechanism for control of matrix degradation.

Results

Loss of TEM8 causes embryonic and postnatal vascular and connective tissue defects

Antxr1 null mice, expressing *LacZ* for localizing *Antxr1* promoter activity, were generated as described in the Methods section. At embryonic days E9.5– E11.5, limb buds, cranial primary vessels, perioptic vascular plexus, cardinal and umbilical veins showed β-galactosidase activity (not shown). At E13.5–14.5 LacZ staining of *Antxr1*−/− whole mount embryos showed strong promoter activity (Figs. 1a and S1b). The perichondrium of all cartilaginous primordia, vibrissae and arteries, including aorta were strongly positive. Extensive hemorrhage found in many *Antxr1*−/− embryos at E11.5 suggested that mutants have defective and leaky vessels (Fig. 1b). Newborn mutant pups did not exhibit any major defects by gross inspection, but homozygous mutants were slightly smaller than heterozygotes and wild-type controls. Homozygous mutants showed progressive growth retardation, bone loss, a shortened skull with frontal bossing and midfacial hypoplasia (Fig. 1c). At 4– 21 weeks, mutant mice had significantly lower body weight than their control littermates (Fig. 1d). Furthermore, *Antxr1* null animals exhibited increased ECM deposition, including fibrosis of various organs and skin (Fig. S1c). Heterozygous knock-in mice, carrying the A-to-T missense change in TEM8, also exhibited growth retardation (Fig. 1e) and increased ECM deposition in skin (Fig. S1d). This is consistent with previous studies indicating that the mutation has a dominant negative effect on TEM8 function [26].

Blood vessel defects and cell signaling alterations in *Antxr1*−/− skin are similar to those in human infantile hemangiomas

In the skin of *Antxr1*−/− animals, intense LacZ activity was found in vessel layers (Fig. 2a). At week 7, these layers contained increased numbers of dilated and leaky vessels as shown by extravasation of perfused FITC-coupled dextran (Fig. 2b). Staining of endothelial cells with lectin showed discontinuous staining with reduced intensity (Fig. 2c). Reduced staining with antibodies against calponin indicated impaired vessel coverage by perivascular cells (Fig. 2c). Similar changes were present but less severe in heterozygous animals. Skin vessels in *Antxr1*−/−animals exhibited increased endothelial cell proliferation and perivascular cell apoptosis. BrdU-labeling indicated greater than 4-fold increase in proliferation of CD31-positive cells and increased numbers of TUNEL-positive CD31-negative cells (Figs. 2d and S2a–c, e–f). A substantial increase in BrdU-labeling was also found in skin from heterozygous knock-in mice (Fig. S2d).

Decreased levels of VEGFR1 and β1 integrin transcripts were found in skin lysates of *Antxr1*−/−mice (7 weeks) by RT-PCR (Fig. 3a). A 3-fold increase in *Vegfa* transcripts, but no changes in other VEGF isoforms, was associated with a 2-fold increase in VEGF plasma levels in *Antxr1*−/− mice (Fig. 3a) and with increased VEGFR2 signaling. Results of western blotting demonstrated that levels of VEGFR1 were decreased, while levels of VEGFR2, phosphorylated VEGFR2, VEGFA and Hif-1α, a downstream target of VEGFR2 signaling, were increased (Fig. 3b). Increased levels of phosphorylated Tie-2 and Angiopoietin 2 indicated that Tie-2 signaling was also affected (Fig. 3b).

Immunohistochemistry showed increased levels of phospho-Erk1/2, indicating that Erk1/2, a downstream effector of VEGFR2 signaling, was activated in mutant vascular cells (Fig. 3c). In addition, examination of skin lysates of *Antxr1*−/− mice (7 weeks) by RT-PCR and ELISA showed increased transcript and protein levels of the Hif-1α target, CXCL12/SDF-1α, increased levels of transcripts for its receptor *Cxcr4*, and increased plasma levels of CXCL12 in *Antxr1*−/−mice compared with WT controls (Fig. 3d). Skin lysates of heterozygous knock-in mice had similar increases in transcript levels for *Vegfa*, *Cxcl12* and *Cxcr4* and increased protein levels of CXCL12 (Fig. 3e).

Loss of TEM8 results in dramatic changes in synthesis of extracellular matrix components in skin and other organs

Analyses of RNA isolated from the skin of 7-week old mice revealed increased transcript levels for collagens type I (*Col1a1*) and type VI (*Col6a1*, *Col6a3*, *Col6a5*, and *Col6a6*), but reduced levels in the case of *Col4a1*, *Col18a1* and *lama5* genes (Fig. 4a). Western blots of total skin lysates showed increased levels of collagen VI and decreased levels of collagen IV (Fig. S3a). Mutant skin sections showed increased staining for collagen I. The staining was predominant in the dermis and especially strong around the hair bulbs and dermal papillae (Fig. 4b). The cutaneous vascular layer of mutant skin showed reduced staining for α1 (XVIII) collagen chains (Fig. S3b). In contrast, collagen VI staining was very strong in the same area (Fig. 4c). Blood vessel walls in mutant skin appeared to be thickened in PAS-stained sections and PAS-stained material was observed in congested vessels (Fig. S3c). Patchy loss of vascular basement membranes and accumulation of collagen fibrils between

endothelial and perivascular cells in mutant skin were observed by electron microscopy (Figs. 4d and S3d).

To determine whether the increased accumulation of collagen in mutant skin may be the result of increased synthesis of collagen in fibroblastic cells, we isolated skin fibroblasts from E17.5 *Antxr1*+/+ and littermate *Antxr1*−/− embryos and compared their incorporation of L-[^{14}C(U)]-Proline into collagen in culture. The results demonstrated a 2-fold increase in the rate of collagen accumulation both in the medium and the cell layer, consistent with increased amounts of pepsin-extracted material from skin of 7-week and 3-month old *Antxr1*−/− mice and increased amounts of α1(I) and α2(I) collagen chains (as determined by gel electrophoresis and mass spectrometry (Figs. 4e,f and S3e)). Dramatic changes in skin morphology, including reduced cellularity, degenerated hair follicles, and increased accumulation of acellular extracellular matrix, were observed in sections from *Antxr1*−/−mutants at 12 weeks (Fig. S3f).

These findings indicate that vascular changes in mutant skin are early (7 weeks) events that are followed by an increasingly severe skin fibrosis over time (12 weeks).To examine the potential contribution of vascular changes to the fibrosis, we examined mice with conditional deletion of *Antxr1* in vascular endothelial cells. The severe skin fibrosis and increased expression of collagens α1(I) and α1(VI) in these conditional mutants clearly indicate that changes in endothelial cells are important parts of the fibrotic mechanism (Fig. 5a, b). Monocytes, macrophages and mast cells are known to play a role in the pathogenesis of fibrosis by secreting profibrotic mediators, such as IL-1, −4, −6, −8, TNF-α, CTGF and TGF-β. Consistent with the increased levels of CXCL12 in mutant animals (Fig. 3d, e), the number of macrophages and mast cells was substantially increased in skin of *Antxr1*−/− mice (Fig. 5c, d). This was associated with increased numbers of interstitial collagen-producing cells, as shown by immunostaining for FSP1, a marker for cells engaged in fibrogenesis (Fig. 5e).

Dysregulated extracellular matrix proteolysis in skin of mutant mice

The data described above indicate that increased synthesis of fibrillar collagen matrix is a major contributor to the fibrosis in TEM8-deficient mice. However, they do not exclude the possibility that the rate of matrix degradation may also be affected. Balance of matrix production with degradation is critical for normal angiogenesis and connective tissue homeostasis. RNA analyses did not show statistically significant differences in transcript levels of the matrix metalloproteinases *Mmp2* and *Mmp9* in the skin of control and mutant animals (Fig. 6a), but immunoblotting revealed increased protein levels of both proteins in mutant skin lysates (Fig. 6b). Immunostaining for MMP9 showed the enzyme to be expressed in the stratum basale of epidermis, the bulge region of hair follicles, sebaceous glands, and in interstitial/dermal cells with monocyte–macrophage morphology (Fig. S4a). MMP2 protein was detected primarily in vascular beds in skin (Fig. S4b). Surprisingly, while the protein level of MMP2 in skin lysates was increased, its activity was dramatically reduced both in *Antxr1*−/− mice and in *Antxr1fl/fl::Cdh5Cre* mice (Figs. 6c, d and S5a). In contrast, the level of active MMP14 was increased (Fig. 6c). RNA analyses indicated that *Timp2* and *Timp3* transcript levels were decreased while *Timp1* transcripts were not changed

(Fig. 6e). Given the positive role of TIMP2 in MMP14-dependent activation of MMP2, it is possible that the low levels of *Timp2* expression may contribute to the lack of MMP2 activity in *Antxr1*−/− skin. However, it is unlikely to be a major factor since MMP2 activity levels were reduced by only 30% in skin lysates of *Timp2*−/− mice (Fig. 6d).

Loss of MMP2 activity requires loss of TEM8 function in both endothelial and fibroblastic cells

Substantial fibrosis, but only about 40% loss of MMP2 activity in mice with conditional deletion of *Antxr1* in endothelial cells, suggests that the almost complete loss of MMP2 activity in skin of *Antxr1*−/−mice requires loss of TEM8 function in both endothelial and non-endothelial cells. To examine the contributions of endothelial and fibroblastic non-endothelial cells to the overall reduction in MMP2 activity, we used three approaches. First, we generated three stable human dermal microvascular endothelial cell (HDMEC) lines with different levels of TEM8 knockdown. The three lines, shTEM8-1, shTEM8-2 and shTEM8-3, had 26%,60% and 90% knockdown of TEM8, respectively (Fig. S5b). The level of TEM8 knockdown correlated with the degree of increase in VEGF levels, both in total cell lysates and in conditioned media (Figs. 7a and S5c). Reducing TEM8 expression resulted in up to 30% reduction of MMP2 activity in lysates of the endothelial cell lines (Figs. 7b and S5d).

Second, we measured the activity of MMP2 in fibroblasts. No difference in the activity of MMP2 was found between WT and mutant fibroblasts isolated from either E17.5 mouse embryos or from the skin of adult mice (data not shown). Third, we assayed for MMP2 activity in an endothelial-fibroblast co-culture system. Co-culture of the human shTEM8-2 or shTEM8-3 endothelial cells with fibroblasts isolated from the skin of adult *Antxr1*−/− mice resulted in dramatic reduction of enzyme activity (Figs. 7c and S5e). Importantly, the level of reduction of MMP2 activity strongly depended on the level of TEM8 knockdown in endothelial cells; no changes in MMP2 enzymatic activity compared with control shTEM8 cells were observed when shTEM8-1 (26% TEM8 knockdown) endothelial cells were co-cultured with murine *Antxr1*−/− or *Antxr1*+/+ fibroblasts (data not shown).

To examine the mechanism by which TEM8-dependent endothelial cell-fibroblast communication results in inactivation of MMP2, we isolated primary CD31-positive ($CD31^+$) and CD31-negative ($CD31^-$) cells in one step from the same sections of mouse skin tissue of 7-week old WT control and *Antxr1*−/− mutant littermates (Fig. S5f). RNA analyses showed that expression levels of *Col1a1* were six-fold higher in control $CD31^-$ than in control $CD31^+$ cells and fivefold higher in mutant than in control $CD31^-$ cells (data not shown), suggesting that the $CD31^-$ cell population represents collagen I-expressing fibroblastic cells. No changes in MMP2 gelatinolytic enzyme activity were observed when WT $CD31^+$ cells were co-cultured with either *Antxr1*−/− or WT $CD31^-$ cells. However, co-cultivation of mutant $CD31^+$ and mutant $CD31^-$cells led to substantial loss of gelatinase activity, whereas co-cultivation of mutant $CD31^+$ cells with WT CD31-negative cells had little effect (Figs. 7d and S5g). To examine whether the effect on MMP2 activation requires cell–cell contact or is due to paracrine signaling, endothelial $CD31^+$ and fibroblastic $CD31^-$ cells were incubated in fibroblast ($CD31^-$) or endothelial ($CD31^+$) cell-conditioned medium

(FCM and ECM, respectively). The MMP2 activity was not affected when WT or mutant $CD31^-$ cells were treated with ECM from WT or mutant $CD31^+$ cells or when WT $CD31^+$ cells were treated with FCM from $CD31^-$ cells. However, the activity was dramatically reduced when mutant $CD31^+$ cells were treated with mutant FCM (Figs. 7d and S5g). Finally, western blotting of total skin lysates as well as lysates of co-cultures of mutant $CD31^+$ and mutant $CD31^-$ cells showed substantial reduction in the level of active (cleaved) form of ADAM17 (Fig. S5h). Since it has been reported that ADAM17 activity is necessary for VEGF-induced MMP-2 activation [27], it is possible that a loss of its activity may contribute to the loss of MMP2 activation.

Experiments in which transcript levels of *Col1a1*, *Col6a1* and *Fn1* were measured in WT and *Antxr1*−/− fibroblasts cultured in conditioned media of $CD31^+$ cells indicated that increased expression of the three matrix genes is primarily a consequence of loss of TEM8 function in fibroblasts (Fig. S5i). *Tnfa* and *Ctgf* expression levels were also increased (data not shown). Taken together, the data indicate that TEM8 functions in both endothelial cells and fibroblasts to control matrix homeostasis and that increased accumulation of extracellular matrix in TEM8-deficient skin is the result of increased synthesis in fibroblastic cells and decreased degradation mediated by MMP2.

Discussion

Vascular and connective tissue homeostasis is maintained by cell–cell and cell–ECM interactions. In vitro and in vivo studies have suggested that ANTXR1/TEM8 may play a role in these interactions [17,28–33]. However, insights into the mechanisms involved have been lacking. For example, in endothelial cells of rapidly growing infantile hemangiomas, clustering of TEM8 with VEGFR2 and β1 integrin is associated with a decrease in VEGFR1 expression and activation of VEGFR2 signaling [26]. Based on the similarities between signaling changes in the skin of TEM8-deficient mice and in endothelial cells isolated from infantile hemangioma patients [26], including a case with the heterozygous TEM8 Ala-to-Thr missense mutation that was knocked into mice as described here, we conclude that TEM8 is essential for regulation of VEGF receptor signaling in vascular endothelial cells. The vascular skin abnormalities in *Antxr1*−/− mice, and presumably in GAPO syndrome patients [30], are not localized as in the lesion of an infantile hemangioma, but are clearly, on a systemic level, reproducing what happens within hemangiomas during their proliferative phase; reduced synthesis of basement membrane components, activation of VEGFR2 signaling associated with low levels of VEGFR1 and increased levels of Hif-1α and its downstream targets CXCL12 and VEGF [34]. As a result, increased numbers of macrophages and mast cells are recruited into the vascular area, both in the skin of *Antxr1*−/− mice and within hemangioma lesions [35]. In turn, this is likely contributing to increased levels of TGF-β1 and CTGF, with the latter being a direct target of Hif-1α as well as a downstream effector of TGF-β1 profibrotic activity [36,37].

The detailed and specific roles of these cellular changes and cytokines during the involution of hemangiomas when the endothelial cells undergo apoptosis and are replaced by fibro-fatty tissue, need further studies. However, our data indicate that the loss of TEM8 function, even when limited to VE-cadherin-expressing cells, results in the production of

profibrogenic growth factors that are capable of stimulating fibroblast activation and collagen production. Such effects, likely mediated by macrophages and mast cells, may contribute to the tissue changes associated with hemangioma involution.

The extracellular matrix changes in the skin of the *Antxr1*−/− mice also provide a mechanistic explanation for the progressive accumulation of extracellular matrix in individuals with the GAPO syndrome [38]. Increased synthesis of matrix proteins, such as fibronectin and collagen types I and VI, is a direct consequence of the lack of TEM8 function in fibroblasts. In addition, our data demonstrate that the breakdown of matrix is compromised in the skin of knockout animals. In spite of increased levels of MMP2 protein and the mature active form of MMP14, increased *Ctgf* expression and reduced expression of *Timp2* in *Antxr1*−/− mice, the proteolytic activity of MMP2 is substantially repressed. Previous studies indicated that CTGF enhances the activation of MMP-2 through an effect on MMP2 protein expression and suppression of TIMP2 [39]. However, it has also been shown that increased levels of fibronectin, as in the case of TEM8-deficient fibroblasts described here, suppress the effect of CTGF on MMP2 activation [40]. It is also well established that TIMP2 is critical for MMP14-dependent activation of pro-MMP2 by serving as an adapter molecule in the MMP2/MMP14/TIMP2 complex [41–45], and we show here that MMP2 activity is reduced in the skin of *Timp2*−/− mice to the same extent as the reduction of activity in the skin of animals with conditional deletion of *Antxr1* in *Cadh5Cre*-expressing cells. Although MMP2 protein is primarily expressed in the vascular region of the skin in *Antxr1*−/− mice, our data indicate that the loss of TEM8 function in both vascular endothelial and fibroblastic cells contribute to the loss of MMP2 activity. First, partial reduction of MMP2 activation occurs when TEM8 levels in endothelial cells are knocked down. Second, MMP2 activity is practically eliminated when *Antxr1*−/− endothelial cells are exposed to conditioned media from *Antxr1*−/− fibroblastic cultures. Importantly, this reduction in activity only occurs when *Antxr1*−/− endothelial cells are exposed to conditioned media from *Antxr1*−/− non-endothelial (fibroblastic) cells; conditioned media from control non-endothelial cells has no effect on MMP2 activity. In addition, no differences in MMP2 activity were observed between lysates of wild type and *Antxr1*−/− fibroblasts. Based on these findings, we hypothesize that fibroblastic *Antxr1*−/− cells secrete a factor that blocks activation of MMP2 produced by endothelial cells. Importantly, this blocking effect is only seen when endothelial cells are TEM8-deficient, suggesting that TEM8 is a regulator of co-operative processes between endothelial and fibroblastic cells. Further studies are required to identify the factors involved. However, studies demonstrating that extracellular Prostate apoptosis response-4 (Par-4) protein is an inhibitor of MMP2 gelatinase activity and that phosphorylation of MMP2 inhibits its activity, suggest that different kinds of inhibitory factors need to be considered [46–48].

The almost complete loss of MMP2 proteolytic activity in the skin of *Antxr1*−/− mice indicates that some of the skin lesions in GAPO syndrome patients are the consequences of pathophysiological mechanisms similar to those that are responsible for skin lesions in a group of osteolysis syndromes (NAO, Torg and Winchester) caused by compound heterozygous or homozygous loss-of-function mutations in MMP2 [23–25]. Local or more widespread accumulation of extracellular matrix components is a characteristic of all the

syndromes, albeit to various degrees. The clinical differences may reflect differences in the involvement of other pathways. For example, since MMP2 activates TGF-β1 by cleaving the latency-associated peptide, the loss of MMP2 activity alone is likely to result in reduced levels of TGF-β1 [49,50]. However, the level of TGF-β1 in skin lysates of *Antxr1*−/− mice is increased and this may contribute to the severe progressive fibrosis in the animals and presumably in GAPO syndrome patients. Whether the skeletal changes in GAPO patients are the consequences of mechanisms similar to those responsible for osteolysis in patients with NAO, Torg and Winchester syndromes, is a question that can only be addressed by further studies of skeletal changes in *Antxr1*−/− mice.

Methods

Generation of *Antxr1* null mice

Generation of null mice (*Antxr1*$^{tm1(KOMP)Vlcg}$) was done through the service provided by the trans-NIH Knock-Out Mouse Project (KOMP); project ID is VG10072. Deletion of 29,703 bases of chromosome 6 (deletion starting at 87, 262, 372 position and ending at position 87, 232,670) results in a frameshift deletion of seven exons (from 2 through 8) and generates a premature stop codon that eliminates synthesis of all ANTXR1/TEM8 transcript variants. Exon 1 in the null allele was replaced by a *TM-LacZ* reporter cassette under the control of *Antxr1* regulatory sequences, allowing spatial and temporal visualization of the pattern of *Antxr1* deletion. Mutant mice were generated using the C57BL6/NTac strain and subsequently crossed into the C57BL6/J strain. Crosses between heterozygous *Antxr1*+/- mice produced progeny of 21% *Antxr1*+/+, 56% *Antxr1*+/- and 23% *Antxr1*−/− pups in 100 analyzed litters. At 4–5 months, the mortality rate of *Antxr1*−/− mice was 35%. In addition, female homozygous knockout mice were infertile and males exhibited impaired reproductive function after 2–3 months. Malocclusion was found in 25% of the homozygotes after 3 months of age.

Generation of *Antxr1* KI mice

Anthrax1 [Mus musculus, Gene ID: NM_054041] gene targeting vector containing the point mutation A324T(GCT/ACT) and fusion of exons E12 and E13 (Fig. S1e), was constructed by Applied StemCell, Inc. and electroporated into a hybrid mouse embryonic stem cell (ESC) line (C57BL6/129SvJ; #ASE-9005).

The neomycin cassette flanked by FRT sites was used as a positive selection marker, while the Diphtheria toxin A fragment cassette (DTA) served as a negative selection marker.

Both 5′ arm and 3′ arm of the targeting vector were designed as homologous arms to introns flanking the E12 and E13, to facilitate homologous recombination. Sequence data were obtained using primer T-SQ1. Sequencing alignment was carried out against that of *Antxr1* vector construct to confirm the deletion of the intron between Exon12 and Exon13, as well as the incorporation of point mutation in Exon13 on the targeted allele (Fig. S1e).

Other mouse lines used

Antxr1 floxed, *Cdh5Cre* (*B6.Cg-Tg*(*Cdh5-cre*)*7Mlia/J*, Jackson Laboratory) and *Timp2 null* mouse lines have been described previously [28,45].

Histology

Dorsal skin samples from 7 week- and 3 month-old *Antxr1*−/− mice and control littermates were collected, fixed overnight in 4% PFA (VWR Int.) at 4 °C and either dehydrated through a graded ethanol series or immersed in 30% sucrose/PBS solution for 24 h at 4 °C prior to paraffin or OCT (Sakura Finetek, USA Int.) embedding and sectioning. For histological examination H&E and Masson's Trichrome staining was used on 5 μm thick sections according to standard protocols. Toluidine blue, pH = 2.2, was used for staining of mast cells.

Western blotting

Western blots were carried out using Abcam western blot protocols. Bullet Blender (BBX24, Next Advance Inc.) and corresponding kit (9–2.0 mm stainless steel bead blend, product number SSB14B and 3.2 mm stainless steel balls in Screw-Cap RINO tubes) were used for homogenization of skin samples. Briefly, lysates were prepared by adding 0.5 ml of pre-chilled (4 °C) M-PER® lysis buffer (mammalian protein extraction buffer, Thermo Scientific) supplemented with proteinase (Roche Applied Science) and phosphatase (Roche Applied Science) inhibitor cocktails to 50–100 mg of frozen tissue and placed in bullet blender lysis kit tubes. For in vitro and ex vivo cell culture analysis, cell lysates were collected using M-PER® buffer supplemented with protease and phosphatase inhibitor cocktail (Roche Applied-Science). After centrifugation, homogenates were transferred to new tubes and left on ice for 30 min before spinning for 30 min at 12,000 rpm in a 4 °C pre-cooled centrifuge. After spinning, supernatants were transferred to fresh tubes kept on ice. Bradford assay (Thermo Scientific) was used to determine protein concentration. Tissue lysates were stored at −80 °C. Lysates containing 10–30 μg of protein were electrophoresed using 5%, 10% or 16% SDS-bispolyacrylamide gels and separated proteins in the gels were transferred to nitrocellulose membranes. After 1 hour blocking at room temperature in 5% milk/TBST (1× PBS, 0.2% Tween-20), blots were incubated overnight at 4 °C with primary antibodies diluted in 4% BSA (Sigma Aldrich)/TBST solution. After washing 3 times for 5 min in TBST, blots were incubated with secondary antibodies for 1 h at room temperature and immunoreactive bands were visualized by chemiluminescent substrate (Thermo Scientific). Secondary antibodies, anti-mouse HRP (1:1000, #32430, Thermo Scientific), anti-rabbit HRP (1:10,000, #31460, Thermo Scientific) and anti-goat HRP (1:5000, sc-2056, Santa Cruz) were diluted in 5% milk/TBST solution. The following primary antibodies were used for western blotting: Flk1 (1:1000, sc-504, Santa Cruz), p-Flk1 (1:1000, sc-101820, Santa Cruz), Flt1 (1:1000, sc-316, Santa Cruz), phospho-VEGFR1 (1:1000, ab62183, Abcam) Tie2 (1:1000, sc-324, Santa Cruz), phospho-Tie2 (1:1.000, ABS219, Millipore), VEGF-A (1:500, sc-152, Santa Crus), p44/42 ERK1/2 (1:1000, #9194, Cell Signaling), phospho-p44/42-ERK1/2 (1:1000, #9101, Cell signaling), S100A4 (1:1000, ab27957, Abcam), α-SMA (1:1000, ab5694, Abcam), Ang1 (1:500, sc-6319 Santa Cruz), Ang2 (1:500, sc-7015, Santa Cruz), MMP2 (1:1000, ab37150, Abcam), MMP14 (1:1000,

GWB-171BC8, GenWay Biotechnology Incorporation), MMP9 (1:1000, AF909, R&D Systems), β-actin (1:5000, A5441, Sigma Aldrich), and CD31 (1:1000, ab28364, Abcam).

Gelatin zymography

For gelatin zymography tissue or cell lysates were mixed with 6× SDS loading buffer (375 mM Tris–HCl pH 6.8, 6% SDS, 48% glycerol, and 0.03% bromophenol blue) without the addition of reducing reagents and boiling; aliquots containing 10 μg of total protein were loaded on 10% bis-acrylamide resolving gel copolymerized with 0.1% of gelatin. After electrophoresis, gels were washed in zymogram renaturing buffer containing 2.5% of Triton X-100 for 2 h and incubated for 24 h (37 °C) in enzyme developing buffer (50 mM of Tris–HCl, pH 7.4; 10 mM of $CaCl_2$; 150 mM of NaCl; 1 μM of $ZnCl_2$ and 0.01% of NaN_3). Staining of gels was done in Coomassie brilliant blue R-250 staining solution (0.5% R-250, 30% methanol and 10% acetic acid) for 2 h followed by the gel distaining procedure. Gelatinolytic bands were quantified with Image J software (http://imagej.nih.gov).

Quantitative real-time PCR

Total RNA was isolated and first strand cDNA was synthesized using iScript (Bio-Rad). Quantitative real-time PCR with a BioRad iCycler® used primers mixed with the iQ™SYBR®Green Supermix (Bio-Rad). Primer sets for *Vegfr1*, *Vegfr2*, *Tie2*, *Itg1*, *Vegf-variants*, *Mmp2*, *Mmp9*, *Timp1*, *Timp2*, *Timp3*, *Col1a1*, *Col6a5*, *Col6a3*, *Col6a1/2*, *Col18a1*, *Col4a1*, *Lama5* and *Gapdh* were purchased from Invitrogen. Primers are listed in Supplementary Table 1. Specificity of reactions was determined by melting curve analysis. The relative fold changes of gene expression between each gene of interest were calculated by standard curve method. For each gene of interest ≥3 independent experiments were performed and each experiment was run in duplicates or triplicates.

ELISA assays

VEGF and CXCL12/SDF-1 protein levels in tissue, plasma, cell lysates and conditional cell medium were assessed using the Quantikine Mouse VEGF- and SDF-1 Immunoassays (R&D Systems) in accordance with the manufacturer's instructions; VEGF and SDF-1 levels in tissue lysates and in lysates from confluent cultures were normalized to protein levels. The optical density of each well was determined using a microplate reader set to 450 nm.

Immunofluorescence

Paraffin or frozen 5 μm sections of skin tissue samples were stained with the following antibodies: CD31 antibody (1:100, ab28364 Abcam) for detection of endothelial cells; Calponin (1:100, EP798Y, Abcam) and α-SMA (1:200, ab5694, Abcam) for detection of perivascular cells, and F4/80 (1:100, ab6640, Abcam) for assessing macrophages in vivo. Collagen type I (1:200, ab21286, Abcam), collagen type IV (1:100, AB756, Chemicon), collagen type XVIII (1:100, sc-32720, Santa Cruz), collagen type VI (1:50, sc-167530, Santa Cruz), and fibronectin (1:500, sc-9068, Santa Cruz) were used for extracellular matrix and basement membrane evaluation. Incubation with primary antibody was followed by

FITC or Texas Red labeled secondary antibody (1:500, Vector Laboratories). Nuclei were stained with Hoechst 33342 fluorescent dye (Thermo Scientific).

FITC-Dextran and FITC-*Lycopersicon esculentum* lectin perfusion

Fluorescein isothiocyanate–dextran (FITC conjugated Dextran, Sigma-Aldrich, FD150) and FITC-*L. esculentum* lectin (Vector Laboratories) were used to assess vessel leakage/integrity according to established protocols. Briefly, after induction of anesthesia the chest cavity of mice was opened, a needle was inserted into the right heart ventricle to allow outflow of blood, and a perfusion cannula was inserted into the left ventricle. The mice were first perfused with PBS, pH 7.4, to wash out erythrocytes, and this was followed by fixative solution containing 1% paraformaldehyde and 0.5% glutar-aldehyde in PBS. The perfusion was followed by 20 μg/ml (FITC)-coupled Dextran or 10 μg/ml FITC-conjugated *L. esculentum* lectin in 1% of Bovine Serum Albumin (BSA, Sigma-Aldrich) in PBS. A perfusion with blocking solution, 3% BSA in PBS was used prior to lectin infusion. Isolated skin tissue samples were post-fixed over night at 4 °C in PFA before being saturated in phosphate-buffered 30% sucrose solution.

Colorimetric immunohistochemistry

Immunohistochemistry with the Vector®NovaRed™ Substrate kit (Vector laboratories Inc.) and VESTASTAIN®*Elite* ABC kit (Vector laboratories Inc.) was performed according to the manufacturer's instructions. Paraffin or frozen 5 μm sections of skin tissue samples were stained with the following antibodies: Phospho- p44/42-ERK (1:100, #9101, Cell signaling), S100A4 (1:500, ab27957, Abcam), MMP2 (1:100, ab37150, Abcam) and MMP9 (1:100, AF909, R&D Systems).

Whole-mount and section staining for β-galactosidase activity

After fixation of mutant and control E13.5 embryos in 0.2% glutaraldehyde in PBS for 30 min at room temperature, embryos were washed three times in rinse solution (0.005% Nonidet P-40 and 0.01% sodium deoxycholate in PBS) and then stained in 5 mM potassium ferricyanide, 2 mM $MgCl_2$, 0.4%β-gal (5-Bromo-4-chloro-3-indolyl β-D-galactopyranoside, B4252 Sigma Aldrich) in PBS for 2–3 h at room temperature followed by 2 times rinse in PBS and post-fixation in 3.7% formaldehyde. Frozen 20 μm sections were mounted on slides and fixed in 0.2% glutaraldehyde in PBS for 10 min on ice. Slides were incubated in detergent rinse solution for 10 min, then stained in β-gal staining solution at 37 °C for 2–3 h and post-fixed in 3.7% PFA for 2 h. Slides were counterstained with Nuclear Fast Red and Eosin solution.

BrdU and TUNEL labeling experiments

Cell proliferation and apoptosis were assessed using BrdU (Zymed®BrdU Staining kit, Invitrogen) and TUNEL (In Situ cell Detection Kit, Fluorescein, Roche-Applied Science) kits. The experiments were performed according to manufacturer's protocols with paraffin or frozen 5 μm sections of skin tissue samples. For BrdU or TUNEL double-labeling, sections were stained with CD31 (BD Pharmingen) or α-SMA antibodies (abcam), followed by BrdU or TUNEL staining.

Collagen isolation

Dorsal skin tissue samples were collected from 7 week- and 3 month-old *Antxr1*−/− mice and control littermates. After brief wash in sterile DPBS (Gibco Life Technologies) tissue samples were immerged in 0.1 M acetic acid for 2 h. After digestion in 0.5 M acetic acid/0.5 mg/ml pepsin solution for 2 days, samples were dialyzed against 0.1 M acetic acid for one day, against 0.1 M NaOH for another day and against Tris-buffer, pH = 7.4, for one more day. All steps were done at 4 °C. Bradford assay was used to determine collagen concentration (mg of collagen/g tissue).

Mass spectrometry

Pepsin-soluble collagen was extracted from the dorsal skin of mutant and control littermates. Following PAGE, the 5% gel was stained with 0.0.5% of R-250 solution in 7.5% methanol/10% acetic acid, followed by destaining of gel to a clear background. Excised gel band(s) were placed in a microcentrifuge tube with 50 μl of water (Millipore Water) and used for LC/MS/MS analysis. Average max intensity (In) of α1(I) and α2(I) protein bands were used to estimate the relative amount of collagen type I. The following formula was used to calculate relative α1(I)/α2(I) (In):

$$\mathrm{Relative}\alpha 1/\alpha 2(\mathrm{I})\mathrm{intensity}=\frac{(\mathrm{max}\ \ \mathrm{average}\ \ \mathrm{In}\alpha 1/\alpha 2(\mathrm{I})/\mathrm{max}\ \ \mathrm{average}\ \ \mathrm{InX})\mathrm{KO}}{(\mathrm{max}\ \ \mathrm{average}\ \ \mathrm{In}\alpha 1/\alpha 2(\mathrm{I})/\mathrm{max}\ \ \mathrm{average}\ \ \mathrm{InX})\mathrm{WT}},$$

where X is the intensity of albumin that was used as an internal reference, KO denotes null, and WT is the wild type.

Electron microscopy

For histological analysis dorsal skin tissue of mutant and wild-type littermates was fixed in 2.5% glutaraldehyde and 1.25% paraformaldehyde in 0.1 M cacodylate buffer (pH 7.4) for one day. After postfixation in 4% osmium tetroxide, and dehydration steps, the skin tissue was embedded in TABB epon (Marivac Ltd., Halifax, Canada). Ultrathin sections were contrasted with uranyl acetate and lead citrate before evaluation in a 1200EX JEOL electron microscope.

Isolation of primary mouse embryonic fibroblasts

Dissected skin from E17.5 embryos was placed in sterile DPBS (Gibco® Life Technologies) supplemented with 1% penicillin and streptomycin (P/S, Gibco® Life Technologies). Minced tissue was transferred into 50 ml tubes containing 5 ml of 1 mg/ml collagenase type II (17101-015 Gibco® Life Technologies) in serum free DMEM (Gibco® Life Technologies) medium and 1% P/S. After incubation in a water-bath shaker for 1 h at 37 °C, 5 ml of trypsin solution was added for the last 10 min of incubation. Trypsin and collagenase activities were quenched by adding 15% FBS (Gibco® Life Technologies). Tissue was broken up by pipetting up and down, passed through 40 μm pore size nylon mesh strainer (BD Falcon) in new tubes, and tubes were centrifuged for 5 min at 300 g at 4 °C. Cell pellets were washed 3 times by centrifugation with DPBS to remove any residual amount of collagenase and trypsin, resuspended in DMEM supplemented with P/S, 1% GlutaMax

(Gibco® Life Technologies) and 15% FBS and evenly plated on gelatin (attachment factor protein, AF, Gibco ® Life Technologies) coated plates. Cells were allowed to grow to confluence and either harvested via trypsinization and frozen for storage or split for experiments. For consistency, passage 3 (P3) cells were used in all the described experiments.

Isolation of primary endothelial cells and fibroblasts from adult mice

Anesthetized mice were perfused with PBS, pH 7.4, to wash out erythrocytes. Dorsal skin tissue samples of 7 week-old mutant and wild type littermates were digested in 1 mg/ml collagenase type II (17101-015 Gibco® Life Technologies) in DMEM or EGM-2 (Gibco® Life Technologies) serum-free medium and P/S solution for isolation of fibroblasts or endothelial cells. Fibroblasts were cultured as described above. Dynabeads containing M-450 sheep anti-rat IgG (Life Technologies), in PBS + 0.1% BSA + 0.02% NaN3 were used to isolate endothelial cells according to manufacturer's instructions. Purified rat anti-mouse CD31 (Pharmingen, #553369), was used to prepare anti-mouse CD31-conjugated Dynabeads by adding 5 μl of anti-CD31 antibody for each 100 μl of beads and incubation overnight at 4 °C.

To isolate $CD31^+$ cells, 30 μl of anti-mouse CD31-coupled Dynabeads was added per 1 ml of cell suspension followed by incubation on a rotator for 1 h at room temperature, followed by separation on a magnetic separator for 1–2 min. The bound $CD31^+$ cells (beads + cells) were cultured in EGM-2 medium, supplemented with growth factors (Lonza) and 20% FBS while the unbound fractions, $CD31^-$ supernatants, were centrifuged for 5 min at 1200 rpm and then resuspended in DMEM medium with 1% of GlutaMax and 15% FBS. CD31-positive and CD31-negative cells were plated in gelatin-coated plates.

Analysis of rate of collagen synthesis

Isolated E17.5 skin fibroblasts from control and mutant mice were plated in 6-well plates at 5×10^5 cells/well density in DMEM (Gibco® Life Technologies) medium supplemented with 1% penicillin and streptomycin and 15% FBS (Gibco® Life Technologies). Upon reaching confluence cells were starved in serum-free medium. After starvation for 24 h, medium was replaced by freshly prepared serum-free DMEM medium containing all non-essential amino acids, except proline (Gibco® Life Technologies); 50 μg/ml of ascorbic acid (Sigma Aldrich) was added to support prolyl hydroxylation and collagen synthesis. To examine the rate of collagen synthesis, cells were pulse-labeled for 6 h in medium containing 1 μCi/ml of L-[^{14}C(U)]-Proline, (50 μCi Perkin Elmer). At the end of the pulse, medium was replaced by regular serum-free medium containing all non-essential amino acids, including proline. Cells and medium were collected at 3 different time points: right after the L-[^{14}C(U)]-Proline pulse and 24 and 36 h after the L-[^{14}C(U)]-Prolinelabeling. Collected samples were kept on ice and proteinase inhibitor cocktail (Roche Applied Science) was added immediately to the collected media. Cells were resuspended in lysis buffer (0.4 M NaCl; 0.1 M Tris–HCl; pH = 7.8 and 1% Triton X-100). After incubation on ice for 3 h, cells were spun in a pre-cooled (4 °C) centrifuge at 1000 rpm for 15 min. Collagenous proteins in supernatants and collected media were precipitated in 30% ammonium sulfate (176 mg $(NH_4)_2SO_4$ were added to each ml of collected supernatant/

medium) by centrifugation at 30,000 rpm for 30 min at 4 °C [51]. Precipitates were dissolved in Tris–HCl buffer (0.4 M NaCl and 0.1 M Tris–HCl buffer, pH = 7.8) in a volume corresponding to 1/50 of initial medium or cell lysate volume. Scintillation fluid was added and samples were mixed vigorously. Incorporation of L-[^{14}C(U)]-Proline was counted in a scintillation counter and rate of collagen synthesis was expressed as DPM L-[^{14}C(U)]-Proline/mg of protein. Blank counts, i.e. DPM of dissolving solution and scintillation fluid, were subtracted from all samples. Two independent experiments (fibroblasts isolated from the skin of E17.5 embryos of 2 controls and 2 knock-outs) were performed in triplicates for each time point.

Generation of stable shTem8 cell lines

Human Dermal Microvascular Endothelial Cells (HDMECs) were used to generate stable lines with *Antxr1* gene knockdown. The cells were treated with TEM8 shRNA Lentiviral Particles (sc-44144 V-V, Santa Cruz), Control shRNA Lentiviral Particles (sc-108080, Santa Cruz), or copGFP Control Lentiviral Particles (sc-108084, Santa Cruz) in the presence of 5 μg/ml Polybrene (sc-134220, Santa Cruz). To select stable clones expressing shRNA, cells were treated with 2 μg/ml puromycin dihydrochloride (sc-108071, Santa Cruz) until resistant colonies were identified and used for subsequent experiments.

Co-culture of fibroblasts and endothelial cells

Primary endothelial cells isolated from skin or stable endothelial cell lines with *Antxr1* gene knockdown were used for co-culture with primary fibroblasts in a 2:1 ratio.

To examine paracrine signaling between fibroblasts and endothelial cells, endothelial cells or fibroblasts were incubated in fibroblast- or endothelial-conditioned medium, respectively. To prepare conditioned media (CM), confluent cells were washed 3 times with PBS, then starved in corresponding serum-free medium for 24 h followed by centrifugation of collected media at 5000 rpm for 10 min and filtration through a 0.45 μm filter to remove cell debris. Freshly prepared CM was used in 1:1 ratio with corresponding complete medium to incubate cells for additional 48 h. Western blotting, RT-PCR, and gelatin zymography were performed after 48 h of cell culturing.

Statistical analysis

Data were analyzed using unpaired 2-tailed Student's *t*-test. All results were expressed as mean ± standard deviation (data from ≥3 independent experiments). Results were considered significant at $P \leq 0.05$.

Study approval of animal use

The described animal experiments were done according to the basic protocols approved by the Harvard Medical Area Standing Committee and in an agreement with the U.S. Public Health Service Policy on Human Care and Use of Laboratory Animals.

Supplementary Material

Refer to Web version on PubMed Central for supplementary material.

Acknowledgments

We thank Nikon Imaging Center, Electron Microscopy facility, Mass Spectrometry and Isotope Counting centers at Harvard Medical School for providing equipment and technical assistance when needed. Authors also thank Sofiya Plotkina for the technical assistance in mouse husbandry and genotyping analysis. We also thank the members of the Olsen laboratory and members of the Program Project for helpful discussions. We are grateful for the service (generation of *Antxr1* null and *Antxr1 KI* mouse strains) provided by the trans-NIH Knock-Out Mouse Project (KOMP) and Applied StemCell, Inc. The work was supported by Program Project grant P01 AR48564 "Molecular and Cellular Mechanisms of Vascular Anomalies" (B.R.O.), a Dean's Scholar Fellowship 2011–2013 (T.Y.B.) and NIH R37DK39773 (J.V.B).

Abbreviations used

GAPO syndrome	autosomal recessive disorder GAPO is an acronym for growth retardation, alopecia, pseudoanodontia and progressive optic atrophy
ECM	extracellular matrix

References

1. Wynn TA. Common and unique mechanisms regulate fibrosis in various fibroproliferative diseases. J Clin Invest. 2007; 117:524–529. [PubMed: 17332879]
2. Strieter RM, Gomperts BN, Keane MP. The role of CXC chemokines in pulmonary fibrosis. J Clin Invest. 2007; 117:549–556. [PubMed: 17332882]
3. Varga J, Abraham D. Systemic sclerosis: a prototypic multisystem fibrotic disorder. J Clin Invest. 2007; 117:557–567. [PubMed: 17332883]
4. Pattanaik D, Brown M, Postlethwaite AE. Vascular involvement in systemic sclerosis (scleroderma). J Inflamm Res. 2011; 4:105–125. [PubMed: 22096374]
5. Castelino FV, Varga J. Emerging cellular and molecular targets in fibrosis: implications for scleroderma pathogenesis and targeted therapy. Curr Opin Rheumatol. 2014; 26:607–614. [PubMed: 25191991]
6. Abraham DJ, Varga J. Scleroderma: from cell and molecular mechanisms to disease models. Trends Immunol. 2005; 26:587–595. [PubMed: 16168711]
7. Maurer B, Distler A, Suliman YA, Gay RE, Michel BA, Gay S, et al. Vascular endothelial growth factor aggravates fibrosis and vasculopathy in experimental models of systemic sclerosis. Ann Rheum Dis. 2014; 73:1880–1887. [PubMed: 23918036]
8. Bradley KA, Mogridge J, Mourez M, Collier RJ, Young JA. Identification of the cellular receptor for anthrax toxin. Nature. 2001; 414:225–229. [PubMed: 11700562]
9. Abrami L, Liu S, Cosson P, Leppla SH, van der Goot FG. Anthrax toxin triggers endocytosis of its receptor via a lipid raft-mediated clathrin-dependent process. J Cell Biol. 2003; 160:321–328. [PubMed: 12551953]
10. Martchenko M, Jeong SY, Cohen SN. Heterodimeric integrin complexes containing beta1-integrin promote internalization and lethality of anthrax toxin. Proc Natl Acad Sci U S A. 2010; 107:15583–15588. [PubMed: 20713715]
11. Young JA, Collier RJ. Anthrax toxin: receptor binding, internalization, pore formation, and translocation. Annu Rev Biochem. 2007; 76:243–265. [PubMed: 17335404]
12. St Croix B, Rago C, Velculescu V, Traverso G, Romans KE, Montgomery E, et al. Genes expressed in human tumor endothelium. Science. 2000; 289:1197–1202. [PubMed: 10947988]
13. Yang MY, Chaudhary A, Seaman S, Dunty J, Stevens J, Elzarrad MK, et al. The cell surface structure of tumor endothelial marker 8 (TEM8) is regulated by the actin cytoskeleton. Biochim Biophys Acta. 1813; 2011:39–49.
14. Nanda A, Carson-Walter EB, Seaman S, Barber TD, Stampfl J, Singh S, et al. TEM8 interacts with the cleaved C5 domain of collagen alpha 3(VI). Cancer Res. 2004; 64:817–820. [PubMed: 14871805]

15. Werner E, Kowalczyk AP, Faundez V. Anthrax toxin receptor 1/tumor endothelium marker 8 mediates cell spreading by coupling extracellular ligands to the actin cytoskeleton. J Biol Chem. 2006; 281:23227–23236. [PubMed: 16762926]
16. Trescos Y, Tournier JN. Cytoskeleton as an emerging target of anthrax toxins. Toxins (Basel). 2012; 4:83–97. [PubMed: 22474568]
17. Vargas M, Karamsetty R, Leppla SH, Chaudry GJ. Broad expression analysis of human ANTXR1/TEM8 transcripts reveals differential expression and novel splizce variants. PLoS One. 2012; 7:e43174. [PubMed: 22912819]
18. Stranecky V, Hoischen A, Hartmannova H, Zaki MS, Chaudhary A, Zudaire E, et al. Mutations in ANTXR1 cause GAPO syndrome. Am J Hum Genet. 2013; 92:792–799. [PubMed: 23602711]
19. Jinnin M, Ishihara T, Boye E, Olsen BR. Recent progress in studies of infantile hemangioma. J Dermatol. 2010; 37:283–298. [PubMed: 20507397]
20. Tipton RE, Gorlin RJ. Growth retardation, alopecia, pseudoanodontia, and optic atrophy—the GAPO syndrome: report of a patient and review of the literature. Am J Med Genet. 1984; 19:209–216. [PubMed: 6507471]
21. Castrillon-Oberndorfer G, Seeberger R, Bacon C, Engel M, Ebinger F, Thiele OC. GAPO syndrome associated with craniofacial vascular malformation. Am J Med Genet A. 2010; 152A:225–227. [PubMed: 20034076]
22. Wajntal A, Koiffmann CP, Mendonca BB, Epps-Quaglia D, Sotto MN, Rati PB, et al. GAPO syndrome (McKusick 23074)—a connective tissue disorder: report on two affected sibs and on the pathologic findings in the older. Am J Med Genet. 1990; 37:213–223. [PubMed: 2248288]
23. Martignetti JA, Aqeel AA, Sewairi WA, Boumah CE, Kambouris M, Mayouf SA, et al. Mutation of the matrix metalloproteinase 2 gene (MMP2) causes a multicentric osteolysis and arthritis syndrome. Nat Genet. 2001; 28:261–265. [PubMed: 11431697]
24. Zankl A, Bonafe L, Calcaterra V, Di Rocco M, Superti-Furga A. Winchester syndrome caused by a homozygous mutation affecting the active site of matrix metalloproteinase 2. Clin Genet. 2005; 67:261–266. [PubMed: 15691365]
25. Zankl A, Pachman L, Poznanski A, Bonafe L, Wang F, Shusterman Y, et al. Torg syndrome is caused by inactivating mutations in MMP2 and is allelic to NAO and Winchester syndrome. J Bone Miner Res. 2007; 22:329–333. [PubMed: 17059372]
26. Jinnin M, Medici D, Park L, Limaye N, Liu Y, Boscolo E, et al. Suppressed NFAT-dependent VEGFR1 expression and constitutive VEGFR2 signaling in infantile hemangioma. Nat Med. 2008; 14:1236–1246. [PubMed: 18931684]
27. Gooz P, Gooz M, Baldys A, Hoffman S. ADAM-17 regulates endothelial cell morphology, proliferation, and in vitro angiogenesis. Biochem Biophys Res Commun. 2009; 380:33–38. [PubMed: 19150341]
28. Cullen M, Seaman S, Chaudhary A, Yang MY, Hilton MB, Logsdon D, et al. Host-derived tumor endothelial marker 8 promotes the growth of melanoma. Cancer Res. 2009; 69:6021–6026. [PubMed: 19622764]
29. Davies G, Rmali KA, Watkins G, Mansel RE, Mason MD, Jiang WG. Elevated levels of tumour endothelial marker-8 in human breast cancer and its clinical significance. Int J Oncol. 2006; 29:1311–1317. [PubMed: 17016666]
30. Chaudhary A, Hilton MB, Seaman S, Haines DC, Stevenson S, Lemotte PK, et al. TEM8/ANTXR1 blockade inhibits pathological angiogenesis and potentiates tumoricidal responses against multiple cancer types. Cancer Cell. 2012; 21:212–226. [PubMed: 22340594]
31. Verma K, Gu J, Werner E. Tumor endothelial marker 8 amplifies canonical Wnt signaling in blood vessels. PLoS One. 2011; 6:e22334. [PubMed: 21829615]
32. Reeves C, Charles-Horvath P, Kitajewski J. Studies in mice reveal a role for anthrax toxin receptors in matrix metalloproteinase function and extracellular matrix homeostasis. Toxins (Basel). 2013; 5:315–326. [PubMed: 23389402]
33. Liu S, Crown D, Miller-Randolph S, Moayeri M, Wang H, Hu H, et al. Capillary morphogenesis protein-2 is the major receptor mediating lethality of anthrax toxin in vivo. Proc Natl Acad Sci U S A. 2009; 106:12424–12429. [PubMed: 19617532]

34. Medici D, Olsen BR. Rapamycin inhibits proliferation of hemangioma endothelial cells by reducing HIF-1-dependent expression of VEGF. PLoS One. 2012; 7:e42913. [PubMed: 22900063]
35. Kleinman ME, Greives MR, Churgin SS, Blechman KM, Chang EI, Ceradini DJ, et al. Hypoxia-induced mediators of stem/progenitor cell trafficking are increased in children with hemangioma. Arterioscler Thromb Vasc Biol. 2007; 27:2664–2670. [PubMed: 17872454]
36. Higgins DF, Biju MP, Akai Y, Wutz A, Johnson RS, Haase VH. Hypoxic induction of Ctgf is directly mediated by Hif-1. Am J Physiol Renal Physiol. 2004; 287:F1223–F1232. [PubMed: 15315937]
37. Leask A, Abraham DJ. TGF-beta signaling and the fibrotic response. FASEB J. 2004; 18:816–827. [PubMed: 15117886]
38. Goloni-Bertollo EM, Ruiz MT, Goloni CB, Muniz MP, Valerio NI, Pavarino-Bertelli EC. GAPO syndrome: three new Brazilian cases, additional osseous manifestations, and review of the literature. Am J Med Genet A. 2008; 146A:1523–1529. [PubMed: 18470892]
39. Yang M, Huang H, Li J, Huang W, Wang H. Connective tissue growth factor increases matrix metalloproteinase-2 and suppresses tissue inhibitor of matrix metalloproteinase-2 production by cultured renal interstitial fibroblasts. Wound Repair Regen. 2007; 15:817–824. [PubMed: 18028129]
40. Droppelmann CA, Gutierrez J, Vial C, Brandan E. Matrix metalloproteinase-2-deficient fibroblasts exhibit an alteration in the fibrotic response to connective tissue growth factor/CCN2 because of an increase in the levels of endogenous fibronectin. J Biol Chem. 2009; 284:13551–13561. [PubMed: 19276073]
41. Itoh Y, Seiki M. MT1-MMP: a potent modifier of pericellular microenvironment. J Cell Physiol. 2006; 206:1–8. [PubMed: 15920734]
42. Nagase H, Visse R, Murphy G. Structure and function of matrix metalloproteinases and TIMPs. Cardiovasc Res. 200669:562–573. [PubMed: 16405877]
43. Shiryaev SA, Remacle AG, Golubkov VS, Ingvarsen S, Porse A, Behrendt N, et al. A monoclonal antibody interferes with TIMP-2 binding and incapacitates the MMP-2-activating function of multifunctional, protumorigenic MMP-14/MT1-MMP. Oncogenesis. 2013; 2:e80. [PubMed: 24296749]
44. Wang Z, Juttermann R, Soloway PD. TIMP-2 is required for efficient activation of proMMP-2 in vivo. J Biol Chem. 2000; 275:26411–26415. [PubMed: 10827175]
45. Caterina JJ, Yamada S, Caterina NC, Longenecker G, Holmback K, Shi J, et al. Inactivating mutation of the mouse tissue inhibitor of metalloproteinases-2(Timp-2) gene alters proMMP-2 activation. J Biol Chem. 2000; 275:26416–26422. [PubMed: 10827176]
46. Rah B, Amin H, Yousuf K, Khan S, Jamwal G, Mukherjee D, et al. A novel MMP-2 inhibitor 3-azidowithaferin A (3-azidoWA) abrogates cancer cell invasion and angiogenesis by modulating extracellular Par-4. PLoS One. 2012; 7:e44039. [PubMed: 22962598]
47. Filipiak K, Kubinski K, Hellman U, Ramos A, de Pascual-Teresa B. Human protein kinase CK2 phosphorylates matrix metallo-proteinase 2 and inhibits its activity. Chembiochem. 2014; 15:1873–1876. [PubMed: 25044410]
48. Sariahmetoglu M, Crawford BD, Leon H, Sawicka J, Li L, Ballermann BJ, et al. Regulation of matrix metalloproteinase-2 (MMP-2) activity by phosphorylation. FASEB J. 2007; 21:2486–2495. [PubMed: 17435175]
49. Yu Q, Stamenkovic I. Cell surface-localized matrix metalloproteinase-9 proteolytically activates TGF-beta and promotes tumor invasion and angiogenesis. Genes Dev. 2000; 14:163–176. [PubMed: 10652271]
50. Wang M, Zhao D, Spinetti G, Zhang J, Jiang LQ, Pintus G, et al. Matrix metalloproteinase 2 activation of transforming growth factor-beta1 (TGF-beta1) and TGF-beta1-type II receptor signaling within the aged arterial wall. Arterioscler Thromb Vasc Biol. 2006; 26:1503–1509. [PubMed: 16690877]
51. Jimenez SA, Dehm P, Olsen BR, Prokop DJ. Intracellular collagen and protocollagen from embryonic tendon cells. J Biol Chem. 1973; 248:720–729. [PubMed: 4684698]

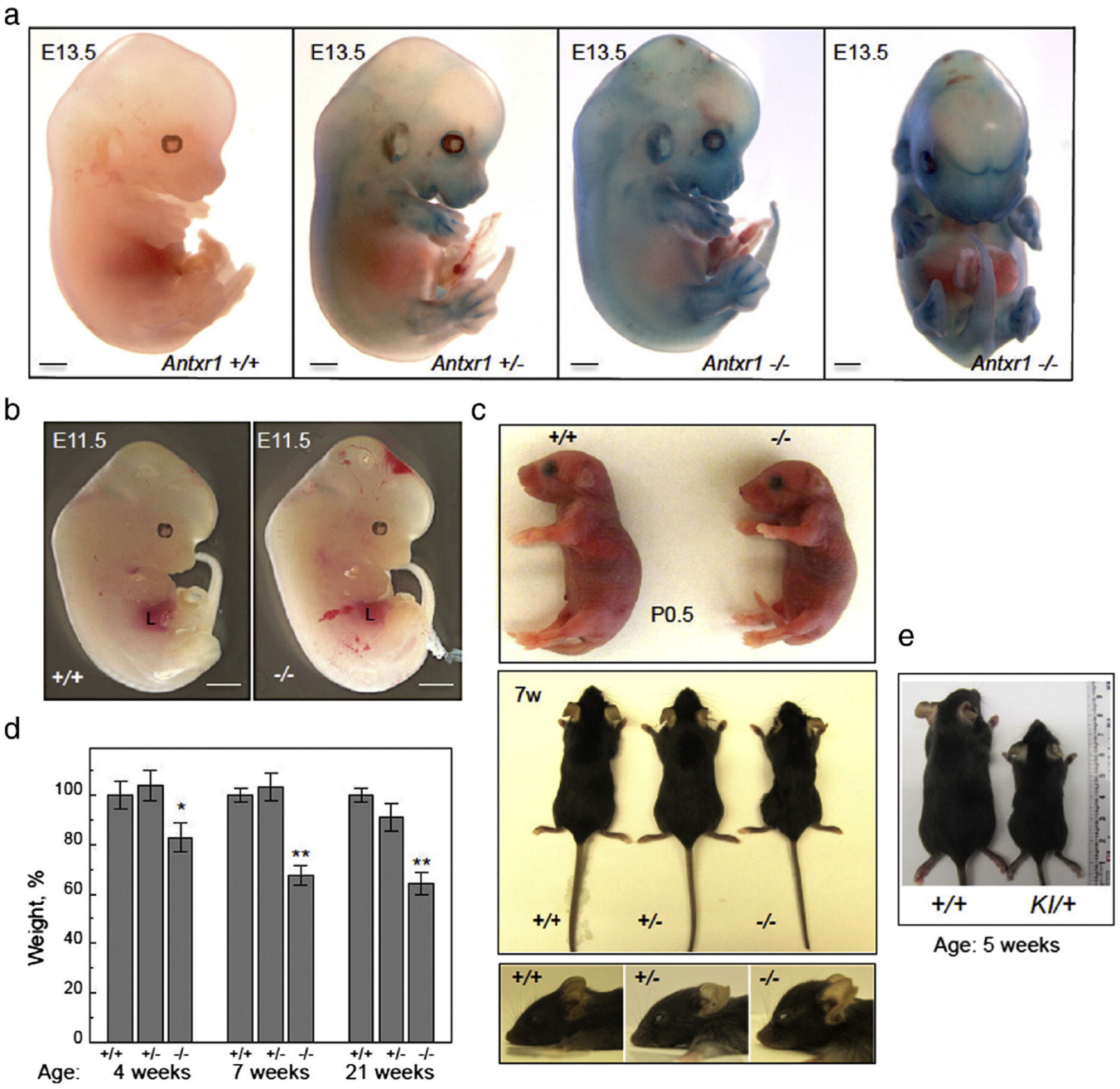

Fig. 1.

Phenotypic characteristics of control and mutant mice. (a) *Antxr1* mutants and control littermates at E13.5, stained for LacZ activity. Scale bars 1 mm. (b) *Antxr1*−/− embryos at E11.5 show evidence of hemorrhage. Liver is indicated by L. Scale bars 1 mm. (c) At birth (P0.5) pups are slightly smaller than wild-type littermates (top). With age (7w(eeks)) mutants show growth retardation and shortened skull with frontal bossing (middle and bottom). (d) Bar graphs showing weight of control and mutant mice at different postnatal ages (n = 10; *P < 0.05, **P < 0.005). (e) Heterozygous knock-in mutant (KI/+) compared with control (+/+) at 5 weeks.

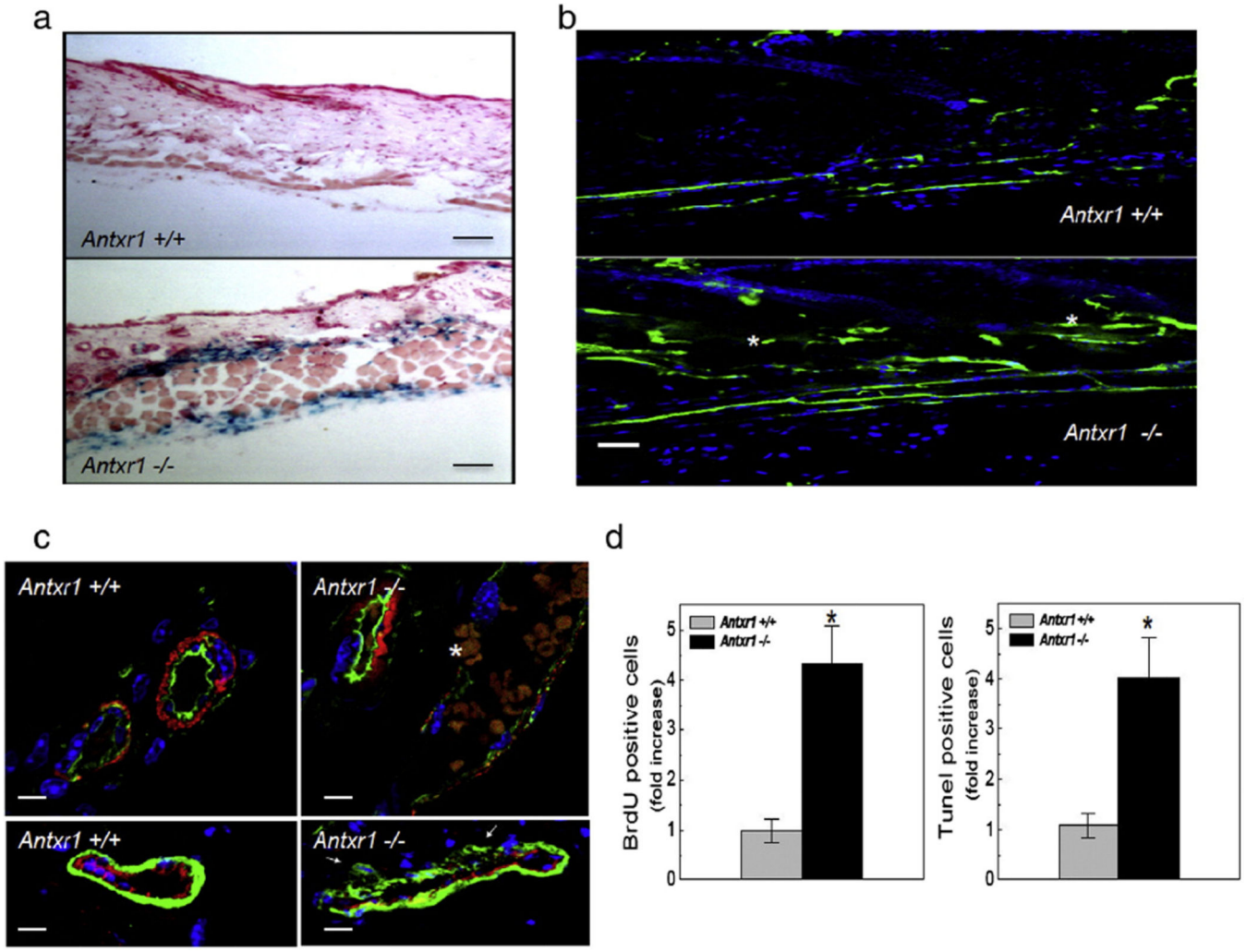

Fig. 2.

Proliferative and leaky cutaneous blood vessels in mutant mice. (a) Strong LacZ staining in cutaneous vessels (20 μm skin sections) of mutant (bottom) compared with control mouse (top) at 7 weeks. Scale bars 100 μm. (b) Immunofluorescence showing extravasation (white stars) of FITC-coupled dextran in skin section of mutant mouse (bottom) compared with control (top). Scale bars 50 μm. (c) Top: Double staining with lectin (green) and antibodies against α-SMA (red); white star at erythrocytes escaping through mutant vessel wall. Bottom: Double immunostaining for endothelial CD31 (red) and perivascular calponin (green) cell markers. White arrows indicate sites of detachment of perivascular cells from vessel wall. Scale bars 25 μm. (d) Bar graphs showing BrdU- and TUNEL-labeling data (n = 10; *P < 0.05). (For interpretation of the references to color in this figure legend, the reader is referred to the web version of this article.)

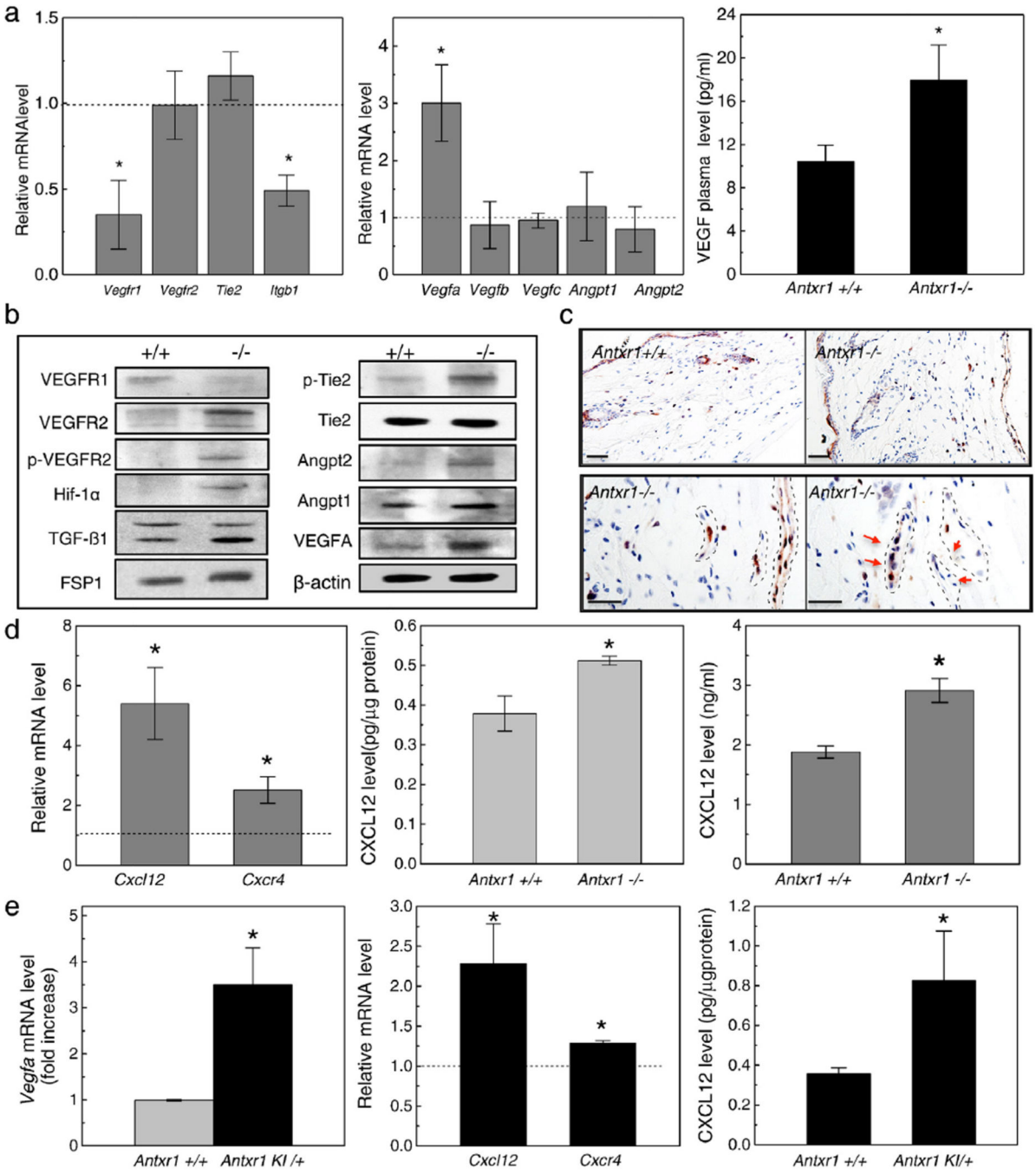

Fig. 3.

Cell signaling changes in skin of mutant mice. (a) Real-time PCR shows reduced transcript levels for *Vegfr1* and *Itgb1* (left) and 3-fold increase in *Vegfa* transcripts (middle) in mutant skin extracts; ELISA shows 2-fold increase in VEGF plasma levels (right) in mutant mice (n = 6; *P < 0.05). (b) Western blots of skin extracts show changes indicative of increased VEGFR2- and Tie2-dependent signaling in mutant mice. (c) Immunohistochemistry of skin sections for phospho-p44/42 MAPK (Erk1/2) shows staining of more cells in mutant mice. Vascular structures indicated by stippled lines in bottom panels. Red arrows indicate mitotic

cells. Scale bars 50 μm (top panels) and 25 μm (bottom panels). (d) Real-time PCR shows increased levels of *Cxcl12* and *Cxcr4* transcripts (left) and ELISA shows increased protein levels of CXCL12 (middle) in mutant skin extracts; ELISA also shows increased CXCL12 levels in plasma (right) of *Antxr1*−/−mice (n = 6; *P < 0.05). (e) Real-time PCR shows increased levels of *Vegfa* (left), *Cxcl12* and *Cxcr4* (middle) and ELISA shows increased CXCL12 protein levels (right) in skin extracts of *Antxr1 KI*/+ mice compared with controls (n = 6; *P < 0.05). (For interpretation of the references to color in this figure legend, the reader is referred to the web version of this article.)

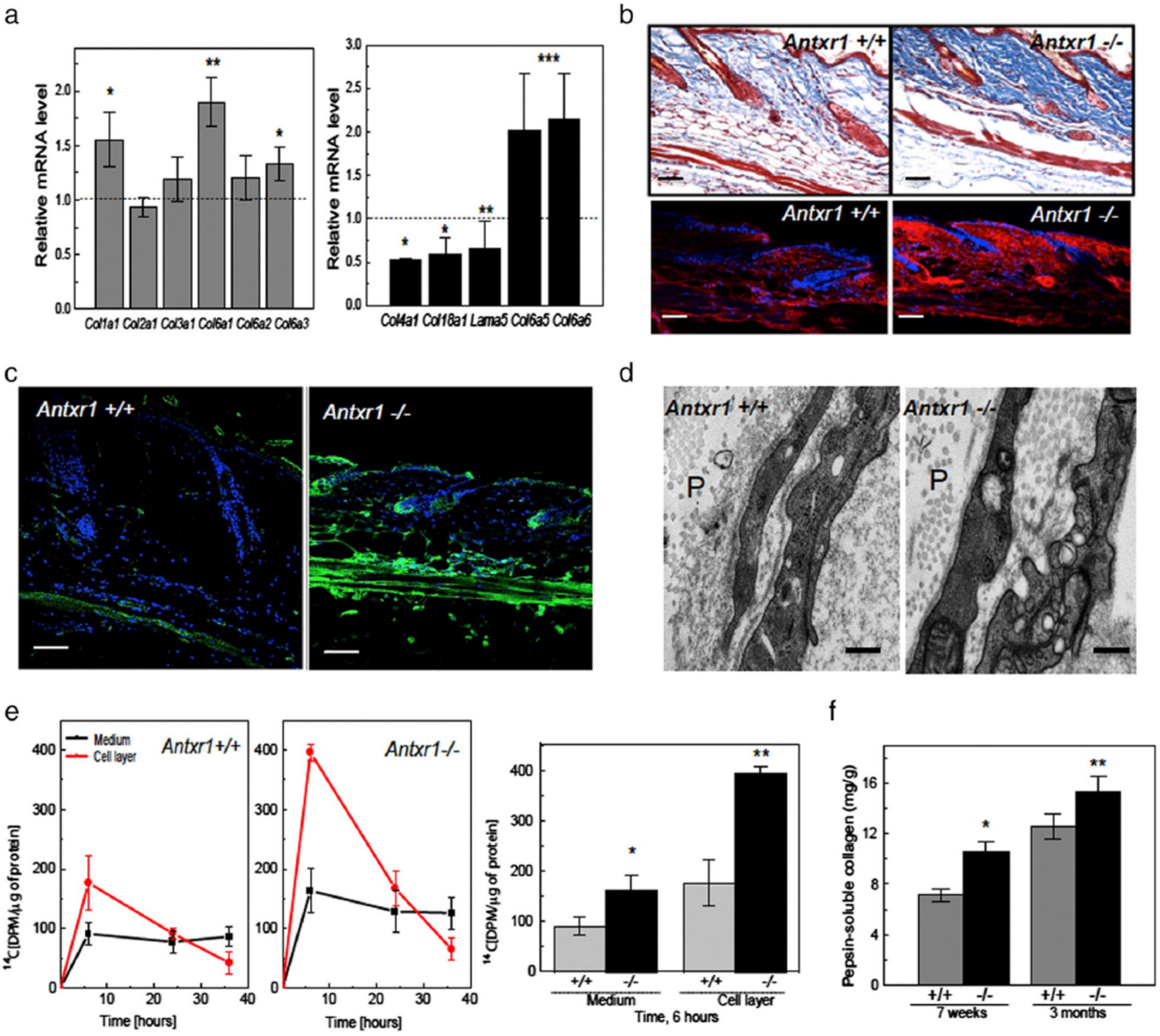

Fig. 4.

Extracellular matrix changes in mutant mice. (a) Increased transcript levels for *Col1a1* and several collagen VI genes, but reduced levels for *Col4a1*, *Col18a1* and *Lama5* in skin extracts of *Antxr1*−/− mice (n = 6; *P < 0.05, **P < 0.005). (b) Histology (top) and immunohistochemistry (bottom) of skin sections show increased collagen deposition and increased levels of α1(I) collagen chains (red) in mutant mice. Scale bars 50 μm. (c) Immunohistochemistry shows increased deposition of collagen VI (green) in mutant skin. Scale bars 50 μm. (d) Electron microscopy indicates loss of vascular basement membranes in mutant mice. Perivascular space indicated by P. Scale bars 500 nm. (e) Left: Radiolabeling with L-[^{14}C(U)]-Proline of collagen synthesized by fibroblasts isolated from control and mutant embryos shows increased incorporation in mutant culture medium and cell layer. Right: Differences between incorporation into collagenous protein at 6 h of

incubation (n = 6; *P < 0.05, **P < 0.005). (f) Increased amounts of pepsin-resistant collagen in skin extracts of mutant mice at 7 weeks and 3 months (n = 4; *P < 0.05, **P < 0.005). (For interpretation of the references to color in this figure legend, the reader is referred to the web version of this article.)

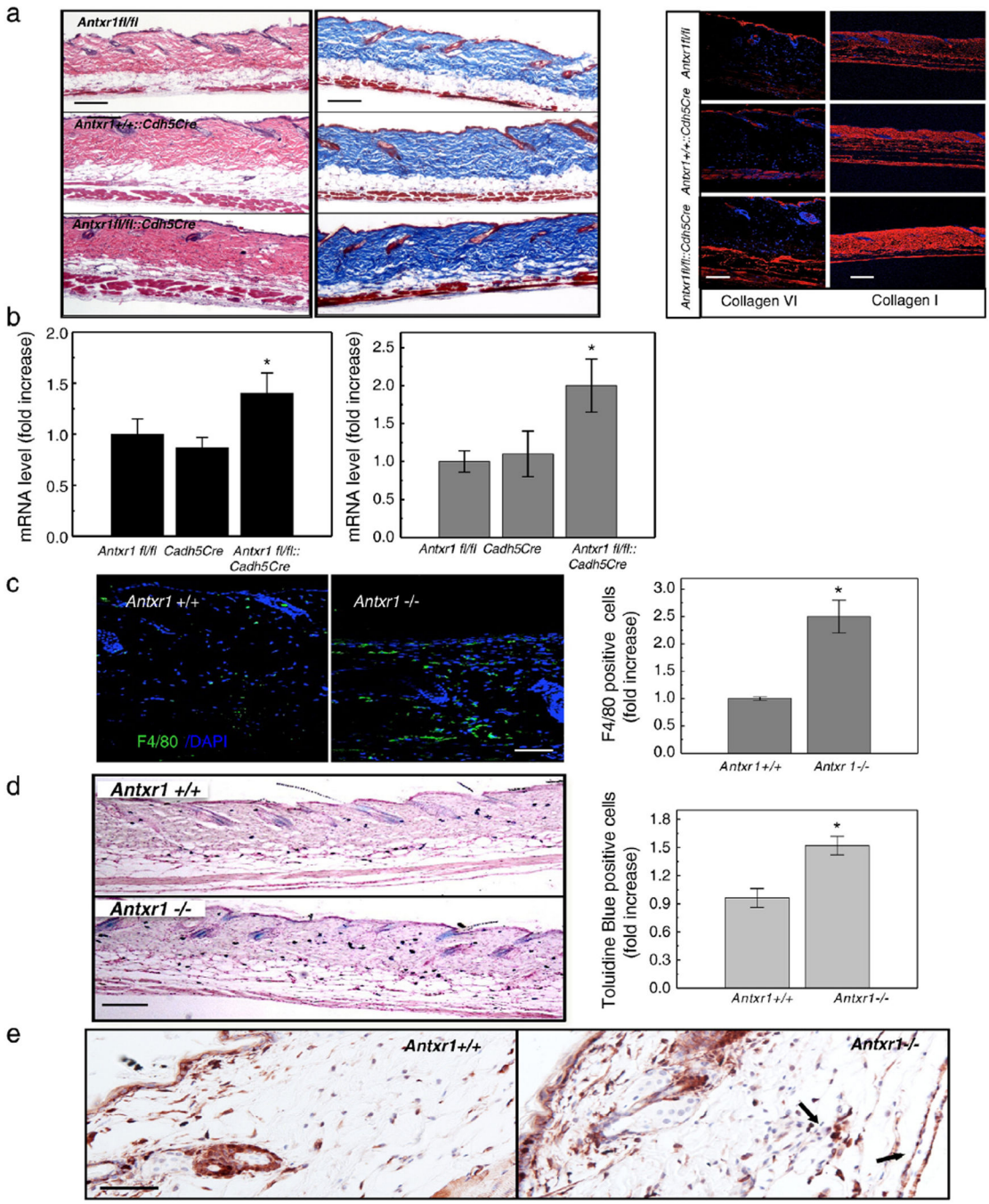

Fig. 5.

Inflammatory cells in mutant skin. (a) Histology of skin sections from control (*Antxr1fl/fl* and *Antxr1+/+::Cdh5Cre*) and homozygous (*Antxr1fl/fl::Cdh5Cre*) conditional knock-out mice (left and middle; scale bar 200 μm); right: immunohistochemical staining for collagens VI (scale bar 100 μm and I (scale bar 200 μm). (b) Increased levels of transcripts for *Col6a1* (left, black bars) and *Col1a1* (right, gray bars) in *Antx1fl/fl::Cdh5Cre* mutant skin (n=4; * $P < 0.05$). (c) Increased numbers F4/80-positive cells (green) in mutant skin. Scale bar 50 μm. (n=9; * $P < 0.05$). (d) Increased numbers of mast cells in mutant skin. Scale bar 200 μm.

(n=10; * $P < 0.05$). (e) Immunohistochemical staining of skin sections for FSP1 demonstrates higher expression in cutaneous vascular regions of *Antxr*−/− mice. Arrows indicate FSP1-positive cells associated with vessels. Scale bars 50 μm.

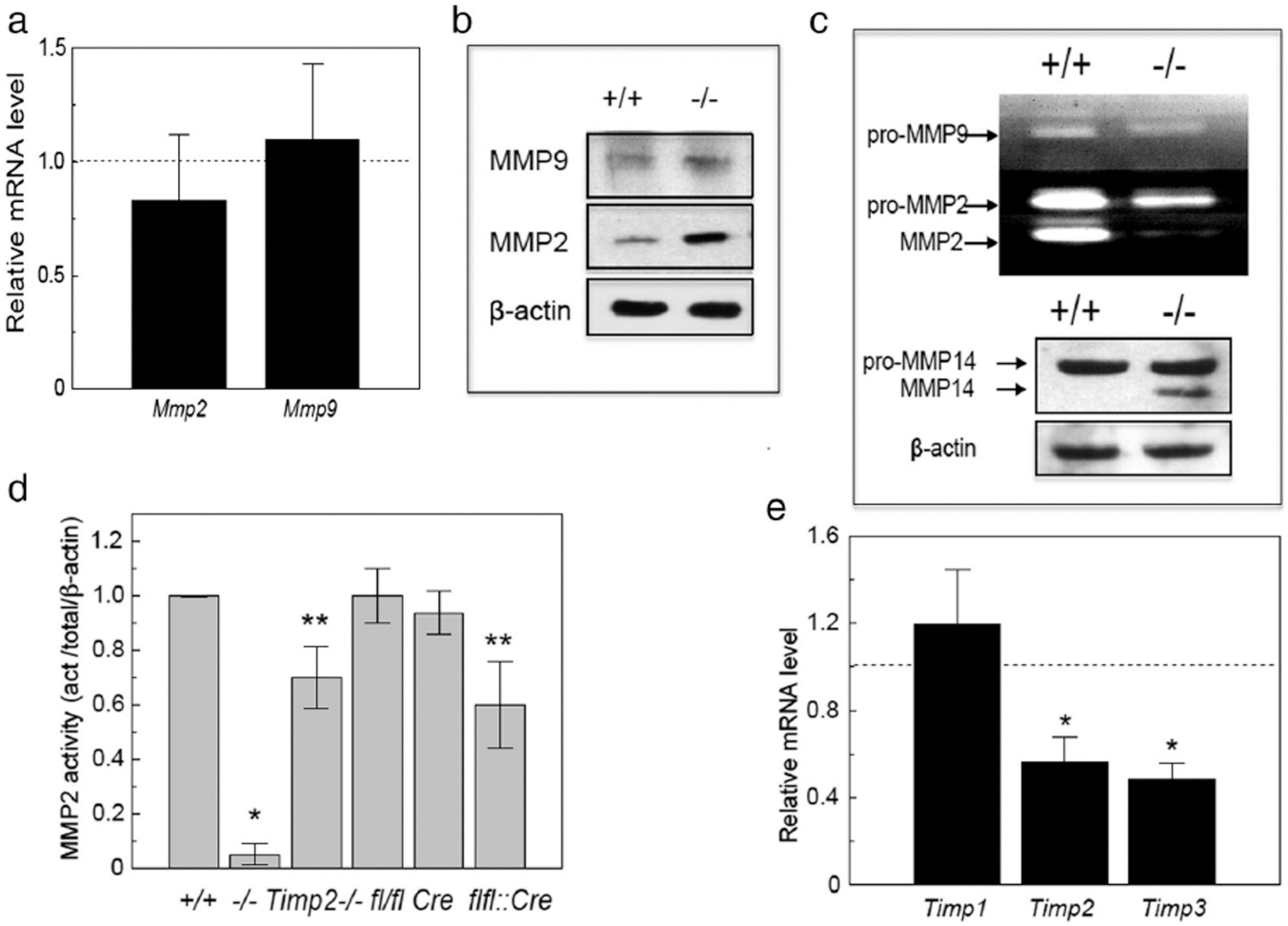

Fig. 6.

MMP changes in skin of mutant animals. (a) Transcript levels of *Mmp2* and *Mmp9* were not affected by loss of *Antxr1* (n ≥ 4). (b) Increased protein levels of MMP9 and MMP2 in skin extracts of *Antxr1*−/− mice. (c) Reduced activity of MMP2 in *Antxr1*−/− mice (top) by gelatin zymography, and increased mature/cleaved form of MMP14 in mutant skin by western blotting (bottom). (d) Reduced MMP2 activity in skin extracts from *Timp2*−/− and *Antxr1fl/fl::Cdh5Cre* (*flfl::Cre*) mice when compared with WT (+/+), *Antxr1fl/fl* (*fl/fl*) or *Cdh5Cre* (*Cre*) control mice, but not to the extent seen in *Antxr1*−/− (−/−) mice (n ≥ 3; *P < 0.05, **P < 0.005). Representative zymography raw data on which this figure is based are shown in Supplemental Fig. 5a. (e) Reduced transcript levels of *Timp2* and *Timp3* in skin extracts from *Antxr1*−/− animals (n = 4; *P < 0.05).

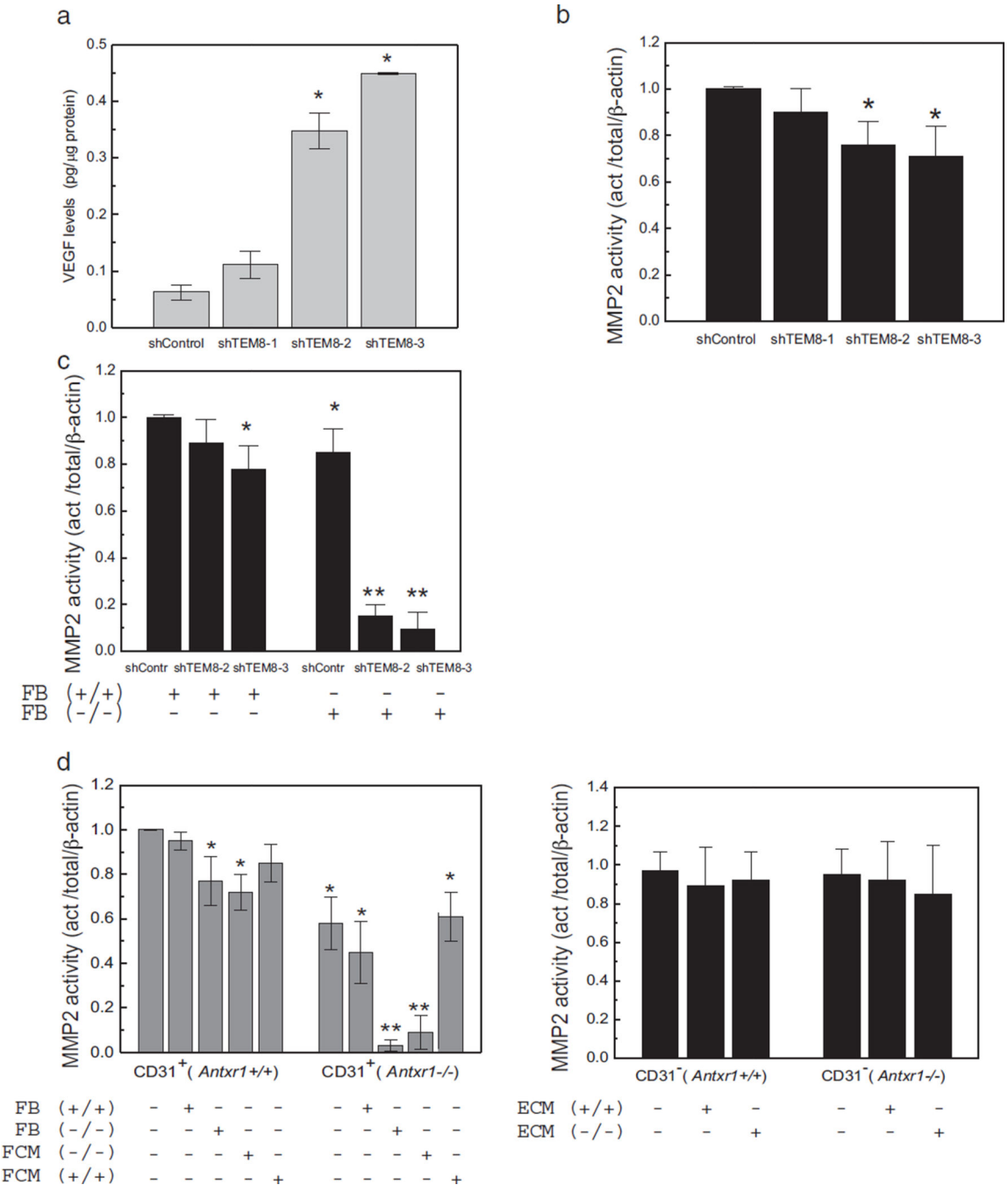

Fig. 7.

Dysregulation of MMP2 activity in TEM8 mutant cells. (a) ELISA showing VEGF levels in lysates of stable endothelial cell lines with different degrees of *Antxr1* knockdown (shTEM8-1/26%; shTEM8-2/60%; shTEM8-3/90%). (n = 3; *P < 0.05). (b) MMP2 activity in lysates of stable endothelial lines with different degrees of *Antxr1* knockdown. (n = 3; *P < 0.05). (c) MMP2 activity is not affected when endothelial *Antxr1* knock-down cells are co-cultured with WT fibroblasts, but is dramatically reduced when the co-cultures contain fibroblasts isolated from *Antxr1*−/− mice. (n ≥ 3; *P < 0.05, **P < 0.005) (d) Left: MMP2

activity in lysates of primary endothelial (CD31-positive) cells from *Antxr1*+/+ and *Antxr1*−/− mice co-cultured with *Antxr1*+/+ or *Antxr1*−/− fibroblasts (FB) or exposed to conditioned medium (FCM) from such fibroblasts. Right: MMP2 activity in lysates of primary fibroblasts (CD31-negative) from *Antxr1*+/+ and *Antxr1*−/− mice cultured with conditioned medium (ECM) from *Antxr1*+/+ or *Antxr1*−/− primary endothelial cells. (n = 3; *P < 0.05, **P < 0.005).